Monthly Notices
of the
ROYAL ASTRONOMICAL SOCIETY
MNRAS **482,** 184–193 (2019) doi:10.1093/mnras/sty2621

The search for high-energy neutrinos coincident with fast radio bursts with the ANTARES neutrino telescope

A. Albert,[1] M. André,[2] M. Anghinolfi,[3] G. Anton,[4] M. Ardid,[5] J.-J. Aubert,[6] J. Aublin,[7] T. Avgitas,[7] B. Baret,[7] J. Barrios-Martí,[8] S. Basa,[9] B. Belhorma,[10] V. Bertin,[6] S. Biagi,[11] R. Bormuth,[12,13] J. Boumaaza,[14] S. Bourret,[7] M. C. Bouwhuis,[12] H. Brânzaş,[15] R. Bruijn,[12,16] J. Brunner,[6] J. Busto,[6] A. Capone,[17,18] L. Caramete,[15] J. Carr,[6] S. Celli,[17,18,19] M. Chabab,[20] R. Cherkaoui El Moursli,[14] T. Chiarusi,[21] M. Circella,[22] J. A. B. Coelho,[7] A. Coleiro,[7,8] M. Colomer,[7,8] R. Coniglione,[11] H. Costantini,[6] P. Coyle,[6] A. Creusot,[7] A. F. Díaz,[23] A. Deschamps,[24] C. Distefano,[11] I. Di Palma,[17,18] A. Domi,[3,25] C. Donzaud,[7,26] D. Dornic,[6★] D. Drouhin,[1] T. Eberl,[4] I. El Bojaddaini,[27] N. El Khayati,[14] D. Elsässer,[28] A. Enzenhöfer,[4,6] A. Ettahiri,[14] F. Fassi,[14] I. Felis,[5] P. Fermani,[17,18] G. Ferrara,[11] L. Fusco,[7,29] P. Gay,[7,30] H. Glotin,[31] T. Grégoire,[7] R. Gracia-Ruiz,[1] K. Graf,[4] S. Hallmann,[4] H. van Haren,[32] A. J. Heijboer,[12] Y. Hello,[24] J. J. Hernández-Rey,[8] J. Hößl,[4] J. Hofestädt,[4] G. Illuminati,[8] C. W. James,[4] M. de Jong,[12,13] M. Jongen,[12] M. Kadler,[28] O. Kalekin,[4] U. Katz,[4] A. Kouchner,[7,33] M. Kreter,[28] I. Kreykenbohm,[34] V. Kulikovskiy,[3,35] C. Lachaud,[7] R. Lahmann,[4] D. Lefèvre,[36] E. Leonora,[37] G. Levi,[21,29] M. Lotze,[8] S. Loucatos,[38,7] M. Marcelin,[9] A. Margiotta,[21,29] A. Marinelli,[39,40] J. A. Martínez-Mora,[5] R. Mele,[41,42] K. Melis,[12,16] P. Migliozzi,[41] A. Moussa,[27] S. Navas,[43] E. Nezri,[9] A. Nuñez,[6,9] M. Organokov,[1] G. E. Păvălaş,[15] C. Pellegrino,[21,29] P. Piattelli,[11] V. Popa,[15] T. Pradier,[1] L. Quinn,[6] C. Racca,[44] N. Randazzo,[37] G. Riccobene,[11] A. Sánchez-Losa,[22] M. Saldaña,[5] I. Salvadori,[6] D. F. E. Samtleben,[12,13] M. Sanguineti,[3,25] P. Sapienza,[11] F. Schüssler,[38] M. Spurio,[21,29] Th. Stolarczyk,[38] M. Taiuti,[3,25] Y. Tayalati,[14] A. Trovato,[11] D. Turpin,[6★†] B. Vallage,[38,7] V. Van Elewyck,[7,33] F. Versari,[21,29] D. Vivolo,[41,42] J. Wilms,[34] D. Zaborov,[6] J. D. Zornoza[8] and J. Zúñiga[8]

Affiliations are listed at the end of the paper

Accepted 2018 September 17. Received 2018 September 15; in original form 2018 July 10

ABSTRACT

In the past decade, a new class of bright transient radio sources with millisecond duration has been discovered. The origin of these so-called fast radio bursts (FRBs) is still a mystery, despite the growing observational efforts made by various multiwavelength and multimessenger facilities. To date, many models have been proposed to explain FRBs, but neither the progenitors nor the radiative and the particle acceleration processes at work have been clearly identified. In this paper, we assess whether hadronic processes may occur in the vicinity of the FRB source. If they do, FRBs may contribute to the high-energy cosmic-ray and neutrino fluxes. A

* E-mail: dornic@cppm.in2p3.fr (DD); dturpin@nao.cas.cn (DT)
† Present address: Key Laboratory of Space Astronomy and Technology, National Astronomical Observatories, Chinese Academy of Sciences, Beijing 100101, China.

search for these hadronic signatures was carried out using the ANTARES neutrino telescope. The analysis consists in looking for high-energy neutrinos, in the TeV–PeV regime, that are spatially and temporally coincident with the detected FRBs. Most of the FRBs discovered in the period 2013–2017 were in the field of view of the ANTARES detector, which is sensitive mostly to events originating from the Southern hemisphere. From this period, 12 FRBs were selected and no coincident neutrino candidate was observed. Upper limits on the per-burst neutrino fluence were derived using a power-law spectrum, $\mathrm{d}N/\mathrm{d}E_\nu \propto E_\nu^{-\gamma}$, for the incoming neutrino flux, assuming spectral indexes $\gamma = 1.0, 2.0, 2.5$. Finally, the neutrino energy was constrained by computing the total energy radiated in neutrinos, assuming different distances for the FRBs. Constraints on the neutrino fluence and on the energy released were derived from the associated null results.

Key words: acceleration of particles – neutrinos – astroparticle physics – radio continuum: transients – methods: data analysis.

1 INTRODUCTION

Discovered in the last decade (Lorimer et al. 2007), fast radio bursts (FRBs) are characterized by a short duration ($t \sim$ a few ms) of intense radio emission (>1 Jy ms) measured so far in the 800-MHz and 1.4-GHz bands by various radio telescopes. The astrophysical origin of FRBs is largely unknown. However, their high dispersion measures (DMs), caused by the scattering of radio waves propagating through an ionized column of matter, suggest an extragalactic/cosmological origin (Lorimer & Kramer 2005; Thornton et al. 2013).

From the 34 FRBs already detected and reported in the FRB catalogue[1] (Petroff et al. 2016), the observed DM can be used to derive upper limits on their cosmological redshift, $z_{\mathrm{DM}} \in [0.12; 2.3]$. This translates into an upper limit on the isotropic radio energy release of $E_{\mathrm{rad}} \in [10^{38}; 10^{41}]$ erg. At present, the FRB progenitors are thought to originate from a large variety of astrophysical sources (Keane et al. 2016), usually split into two classes: repeating sources and single cataclysmic events. For the latter class, the fact that such a large amount of energy is released on a millisecond time-scale may imply that the progenitor does not survive afterwards (single-burst model). Several models have been proposed, such as neutron star mergers (Totani 2013; Wang et al. 2016) possibly associated with short gamma-ray bursts (GRBs) (Zhang 2014; Palaniswamy et al. 2014; Murase Mészáros & Fox 2017) or supramassive neutron star collapses (Falcke & Rezzolla 2014; Ravi & Lasky 2014; Li et al. 2014). Non-destructive flaring models, including giant pulses from young and rapidly rotating neutron stars (Pen & Connor 2015; Cordes & Wasserman 2016), magnetar giant flares (Popov & Postnov 2013; Lyubarsky 2014), hyperflares from soft gamma-repeaters (Popov & Postnov 2010), outbursts from young neutron stars embedded in a wind bubble (Murase Kashiyama & Mészáros 2016) or maybe from the interior of young supernovae (Bietenholz & Bartel 2017) are, however, good astrophysical candidates to explain both repeating and non-repeating FRBs. More exotic models have also been proposed, such as the radio burst radiation of superconducting cosmic strings (Cao & Yu 2018; Ye et al. 2017).

Recently, the discovery of the repeating behaviour of FRB 121102 (Spitler et al. 2016; Scholz et al. 2016) has brought new insights into the nature of FRB progenitors. In addition, radio interferometric observations of FRB 121102 (Marcote et al. 2017; Chatterjee et al. 2017) made it possible, for the first time, to unambiguously determine the redshift of the FRB source at $z \sim 0.19$ (Tendulkar et al. 2017), confirming the tremendous amount of radio energy that can be released during an FRB event.

Radio observation campaigns have been carried out to search for other FRB 'repeaters' among the known FRB population, but without success (Lorimer et al. 2007; Ravi Shannon & Jameson 2015; Petroff et al. 2015a, 2017). However, the instrumental sensitivities and the short observation time of a few hours may account for this null result. Therefore, the question whether or not FRB 121102 belongs to a special class of FRBs is still under debate.

The spatial distribution and the all-sky rate of FRBs, R_{FRB}, can provide additional constraints on the nature of the FRB progenitors when they are compared with distributions and rates of known astrophysical sources. The all-sky rate $R_{\mathrm{FRB}} \sim 10^3\ \mathrm{d}^{-1}$ has been estimated for radio pulses with $F > 1$ Jy ms (Champion et al. 2016). This high event rate would already rule out a short-GRB-dominated population of FRBs, because $R_{\mathrm{FRB}}/R_{\mathrm{short\,GRB}} \sim 10^3$ assuming that $R_{\mathrm{short\ GRB}} = (N_{\mathrm{short\ GRB}}/N_{\mathrm{all\ GRB}})\, R_{\mathrm{GRB}}$, where $R_{\mathrm{all\,GRB}} = 1000\ \mathrm{yr}^{-1}$ in the entire sky and the detected GRB population is composed of one-third of short GRBs according to CGRO-BATSE observations (Goldstein et al. 2013). Alternatively, R_{FRB} corresponds to only 10 per cent of the observed core collapse supernova (CCSN) rate (Thornton et al. 2013). Therefore, the CCSN reservoir may account for the high event rate of FRBs. For instance, Falcke & Rezzolla (2014) claimed that only 3 per cent of the CCSNe producing supramassive neutron stars are needed to explain the FRB rate. The various models proposed are difficult to discriminate because of the lack of additional information on the broadband FRB spectra. Many multiwavelength follow-ups have been organized recently (Petroff et al. 2015b, 2017; Scholz et al. 2017; Bhandari et al. 2018; Hardy et al. 2017), but no counterpart (optical/X-rays/gamma-rays/VHE gamma-rays) has yet been identified. In 2016, however, DeLaunay et al. (2016) reported the detection of a gamma-ray GRB-like counterpart in association with FRB 131104, but with a small significance ($3.2\,\sigma$). For FRB 131104, DeLaunay et al. (2016) determined that the radio-to-gamma-ray energy output ratio would be $E_{\mathrm{rad}}/E_\gamma > 10^{-9}$, assuming that the source is at the redshift inferred by the DM measurement. This may show that a large fraction of the total energy radiated during these radio bursting events may be emitted at high energy while still being undetected or only marginally detected. If the radio emission is likely to be produced by the coherent emission of leptons (Katz 2014, and references therein), then hadronic processes may be the source of the most energetic photons in the gamma-ray energy domain. In this case, TeV–PeV neutrinos could be produced by photo-hadronic interactions. These hadronic processes may occur in the energetic outflow released during a cat-

[1] See the FRB catalogue: http://frbcat.org/

aclysmic FRB event (Falcke & Rezzolla 2014) or in the vicinity of the FRB progenitor through the interaction of the outflow with the surrounding environment (Zhang et al. 2003; Li et al. 2014; Murase et al. 2016; Dey Ray & Dam 2016).

Based on their high rate, $R_{\rm FRB}$, and under the assumption that a fraction of FRBs are indeed efficient accelerators of TeV–PeV hadrons, they may contribute significantly to the cosmic diffuse neutrino signal discovered by the IceCube Collaboration (Aartsen et al. 2013, 2015a,b,c, 2016). This diffuse astrophysical neutrino signal is now established with a high significance. The ANTARES neutrino telescope also observes a mild excess over the background of neutrino candidates at high energies (Albert et al. 2018). To date, no population of astrophysical sources has clearly emerged from the background to explain this diffuse flux. Recently, however, the IceCube Collaboration claimed to have found evidence of a high-energy neutrino signal from the blazar TXS 0506 + 056 (Aartsen et al. 2018a,b), a finding that marks another step towards the identification of the nature of cosmic accelerators in the Universe. Multi-messenger observations of FRBs are crucial if these objects are to be investigated as cosmic accelerators. To date, neutrino searches from FRBs by the IceCube (Fahey et al. 2017; Aartsen et al. 2018c) and the ANTARES (Albert et al. 2017a) Collaborations have yielded a null result.

In this paper, a search for neutrinos in coincident with FRBs detected between 2013 and 2017 using the ANTARES neutrino telescope is presented. Located in the Mediterranean Sea, ANTARES is the largest high-energy neutrino telescope in the Northern hemisphere and has been operating since 2008 (Ageron et al. 2011). By design, the ANTARES detector continuously monitors, with a high-duty cycle and good angular resolution, the Southern sky (2π steradian at any time), where most of the FRBs have been discovered to date. In Section 2, the FRB sample used in the analysis is described, as well as the results of the search for neutrino counterparts. The constraints on the neutrino fluence and energy emission are given in Section 3. Finally, in Section 4, the results are discussed with respect to different expectations from FRB hadronic models and the FRB contribution to the diffuse neutrino flux. Some conclusions are drawn in Section 5.

2 SEARCH FOR HIGH-ENERGY NEUTRINOS FROM FRBS IN THE ANTARES DATA

2.1 The FRBs in the field of view of ANTARES

This analysis focuses on the period from 2013 January to 2017 January, during which 16 FRBs[2] were detected by the Parkes telescope, UTMOST and ASKAP. When active, the ANTARES telescope monitors the sky region with declinations $\delta < -48^\circ$ with an almost 100 per cent duty cycle; for $-48^\circ < \delta < +48^\circ$ the duty cycle decreases gradually because of the requirement that the neutrino candidates are upgoing. The first selection criterion is that the FRB position must be within the ANTARES field of view (FoV) within a chosen time window $\Delta T = [T_0 - 6\text{h}; T_0 + 6\text{h}]$, where T_0 is the FRB trigger time. Three FRBs did not fulfil this first selection criterion and were removed from the sample used in this analysis. In addition, the quality of the ANTARES data acquired during the whole day around each FRB detection was verified to avoid any anomalous behaviour of the detector. One more FRB (FRB 150610) was excluded because the detector was not active owing to a power cut that occurred 4 h before the trigger time. The final sample comprises 12 FRBs for which ANTARES data were considered. Table 1 summarizes the main properties of the FRB sample, and a sky map of the FRB positions superimposed on the ANTARES sky visibility is shown in Fig. 1.

[2]During the review of this paper, a 17th FRB (FRB 141113) was reported by Patel et al. (2018). Occuring in 2014, FRB141113 was below the ANTARES horizon for up to 2 h after its trigger time.

Table 1. Properties of the 12 FRBs visible by ANTARES in the period 2013–2017 according to the FRB catalogue (Petroff et al. 2016). $z_{\rm DM}$ corresponds to the upper limit on the cosmological redshift inferred from the dispersion measure calculated in excess to the Galactic contribution.

FRB	$z_{\rm DM}$	T_0 [UTC]	RA [°]	Dec. [°]	Radio telescope
131104	0.59	18:04:11.20	101.04	− 51.28	Parkes
140514	0.44	17:14:11.06	338.52	− 12.31	Parkes
150215	0.55	20:41:41.71	274.36	− 4.90	Parkes
150418	0.49	04:29:06.66	109.15	− 19.01	Parkes
150807	0.59	17:53:55.83	340.10	− 55.27	Parkes
151206	1.385	06:17:52.78	290.36	− 4.13	Parkes
151230	0.76	16:15:46.53	145.21	− 3.45	Parkes
160102	2.13	08:28:39.37	339.71	− 30.18	Parkes
160317	0.70	09:00:36.53	118.45	− 29.61	UTMOST
160410	0.18	08:33:39.68	130.35	6.08	UTMOST
160608	0.37	03:53:01.09	114.17	− 40.78	UTMOST
170107	0.48	20:05:45.14	170.79	− 5.02	ASKAP

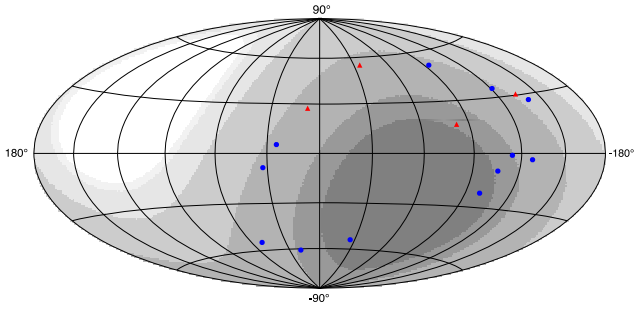

Figure 1. Sky map in Galactic coordinates showing the positions of the 16 FRBs detected in the period 2013–2017. The 12 selected FRBs are shown with blue dots, while the 4 non-selected FRBs are depicted with red triangles. The region of the sky observable by ANTARES (on average) is also displayed in grey-scale, from 100 per cent of visibility for the darkest area to 0 per cent for the white area when considering upgoing neutrino candidates in the detector.

2.2 Method

For each selected FRB, the ANTARES data set was extracted within a time window $\Delta T = [T_0 - 6\text{h}; T_0 + 6\text{h}]$. This time window was chosen to encompass various delay scenarios between the radio and the neutrino signals while keeping the background noise at a low level. Within ΔT, the event rates were checked to verify the detector stability. No significant time variability of the counting rates was found, which ensures the quality of the extracted data. The search for a significant neutrino flux was then based on the detection of upgoing neutrino-induced muons coincident with the position of the FRB within ΔT.

In order to suppress the atmospheric muon background contamination in the neutrino sample, selection cuts were applied using

the quality variables of the track reconstruction algorithm (Adrián-Martínez et al. 2012): the reconstructed zenith angle, θ; the error estimate on the reconstructed direction, β; and the quality fit parameter, Λ. Each selected upgoing ($\cos\theta > 0$) event was required to have a direction error $\beta < 1^\circ$. The final selection criterion was based on the quality fit parameter Λ. For ΔT centred on each FRB time, the optimal value, $\Lambda_{3\sigma}$, was chosen in such a way that the presence of one neutrino candidate in the time window would correspond to a positive signal with 3σ significance (Albert et al. 2017b). Finally, a search cone of 2° was set around each FRB position. From radio information, the typical localization errors correspond to radii of 10 arcmin.

2.3 Results

No upgoing events spatially and temporally correlated with the 12 selected FRBs were found. This null result is compatible with the background event rate of ANTARES, estimated to be $\sim 5 \times 10^{-8}$ event s^{-1}. Because no neutrino signal was detected in coincidence with any of the selected FRBs, constraints on the fluence of neutrinos that would have been observed by the ANTARES detector were derived.

3 CONSTRAINTS ON THE NEUTRINO FLUENCE AND ENERGY EMISSION FROM FRBS

3.1 Constraints on the per-burst neutrino fluence

An upper limit on the neutrino fluence was computed on a per-burst basis with the following procedure. For a given neutrino flux, the number of expected events, N_ν, depends on the detector effective area, $A_{\rm eff}(E_\nu, \delta)$ (units: cm^2). Once the selection parameters ($\cos\theta$, β, $\Lambda_{3\sigma}$) have been defined, as explained in Section 2.2, the effective area depends only on the neutrino energy, E_ν, and the source declination, δ. In order to compute the effective area at any declination, dedicated Monte Carlo simulations reproducing the ANTARES data taking conditions at the FRB trigger time, T_0, were produced.

For a given time-integrated neutrino flux, $\mathrm{d}N/\mathrm{d}E_\nu$ (units: GeV^{-1} cm^{-2}), the number of expected neutrino events for a source at declination δ is

$$N_\nu(\delta) = \int_{E_\nu} A_{\rm eff}(E_\nu, \delta)\, \frac{\mathrm{d}N}{\mathrm{d}E_\nu}\, \mathrm{d}E_\nu \,. \quad (1)$$

Usually, a neutrino power law $\mathrm{d}N/\mathrm{d}E_\nu \propto E_\nu^{-\gamma}$ is assumed. The neutrino fluence at the detector can thus be defined as

$$E_\nu^2 \frac{\mathrm{d}N}{\mathrm{d}E_\nu} = \phi_0 \left(\frac{E_\nu}{E_0}\right)^{-\gamma+2} \quad (\text{in GeV cm}^{-2}) \,. \quad (2)$$

The normalization factor, ϕ_0, has the same units as the neutrino fluence and it corresponds to the expected neutrino energy fluence at the reference energy, $E_0 = 100$ TeV. Owing to the strong energy dependence of the effective area on E_ν, the sensitivity of the detector to a given neutrino flux is strongly dependent on the spectral index γ. Because the neutrino production mechanisms for FRBs are unknown, three spectral models have been tested in this analysis to conservatively cover a large range of possibilities: a hard spectrum with $\gamma = 1.0$, usually considered in some stages of pγ acceleration processes; an intermediate spectrum with $\gamma = 2.0$, corresponding to the theoretical index for Fermi acceleration processes; and a softer spectrum with $\gamma = 2.5$. The latter almost corresponds to the best-fit value of the isotropic astrophysical neutrino signal measured by IceCube (Aartsen et al. 2015b).

By inverting equation (1), a null neutrino detection can be translated to an upper limit on the normalization factor ϕ_0 of the energy spectrum for the given values of the spectral index γ. Assuming Poisson statistics, the 90 per cent confidence level (CL) upper limit, $\phi_0^{90\%}$, is defined by setting $N_\nu(\delta) = 2.3$. No neutrino event was observed in temporal coincidence within $T_0 \pm 6$h for any of the considered FRBs. The values of $\phi_0^{90\%}$ for each FRB and for the three assumed spectral indexes are reported in Table 2.

Starting from the upper limit on the normalization factor, the corresponding 90 per cent CL upper limits on the fluence for each FRB have also been computed, as

$$F_\nu^{90\%} = \int_{E_{\rm min}}^{E_{\rm max}} E_\nu \frac{\mathrm{d}N}{\mathrm{d}E_\nu}\, \mathrm{d}E_\nu = \phi_0^{90\%}\, E_0^{\gamma-2} \int_{E_{\rm min}}^{E_{\rm max}} E_\nu^{1-\gamma}\, \mathrm{d}E_\nu \,. \quad (3)$$

The integration is over the range from $E_{\rm min}$ to $E_{\rm max}$, which corresponds to the energies that define the 5–95 per cent range of the energy distribution of simulated events passing all the analysis cuts for the corresponding spectrum.

The upper limits on the neutrino fluence, $F_\nu^{90\%}$, for each individual FRB and for the three test spectral indexes are reported in Table 2 and shown in Fig. 2. As shown later in Fig. 5, compared with a time-integrated neutrino point-source analysis (e.g. Albert et al. 2017c), searching for neutrinos from short transient events permits us to improve the upper limit derived on the neutrino fluence by a factor of $\sim$30 per cent.

3.2 Constraints on the TeV–PeV neutrino energy released by FRBs

The isotropic neutrino energy, $E_{\nu,\rm iso}$, possibly released during an FRB event is an important physical property of the bursting source. It may provide information on the baryonic load within the ejected outflow as well as on the efficiency of the hadronic processes at work in the acceleration site near the progenitor source. It can be expressed as

$$E_{\nu,iso} = \frac{4\pi D(z)^2}{1+z} F_\nu, \quad (4)$$

where z is the redshift of the source and $D(z)$ is the distance travelled by the neutrinos, which in turn depends on the assumed cosmological model:

$$D(z) = \frac{c}{H_0} \int_0^z \frac{(1+z')\mathrm{d}z'}{\sqrt{\Omega_m (1+z'^3) + \Omega_\Lambda}}, \quad (5)$$

where c is the velocity of light in a vacuum and the cosmological parameters are $H_0 = 67.8$ km s^{-1} Mpc^{-1}, $\Omega_m = 0.308$ and $\Omega_\Lambda = 1 - \Omega_m$ (Ade et al. 2016). For distances in the range d $\in$ [1 kpc ; $D(z_{\rm DM})$], the 90 per cent CL upper limits on $E_{\nu,\rm iso}$ have been computed, and the results are shown in Fig. 3 for each FRB. The excluded region in the $E_{\nu,\rm iso}$–$D(z)$ plane for the hardest considered spectrum ($\gamma = 1.0$) and the softest spectrum ($\gamma = 2.5$) are also indicated. The per burst constraints on $E_{\nu,\rm iso}$ obtained with the power-law spectrum $\gamma = 2.0$ is similar to that obtained with $\gamma = 2.5$, as the two corresponding $F_\nu^{90\%}$ are similar.

Because the distances of these FRBs are unknown, three distance scenarios can be assumed, in which the sources are: (i)

Table 2. The 90 per cent confidence level upper limits on the spectral fluence, $\phi_0^{90\%}$, evaluated at 100 TeV, and the fluence, $F_\nu^{90\%}$, for the three spectral models considered in this analysis ($\gamma = 1.0, 2.0, 2.5$). $\phi_0^{90\%}$ and $F_\nu^{90\%}$ are expressed in GeV cm^{-2}. The [5%; 95%] energy boundaries, $E_{\rm min}$ and $E_{\rm max}$, used to compute the energy-integrated fluence are also shown, in units of $\log_{10}(E_\nu/{\rm GeV})$.

	$\gamma = 1.0$				$\gamma = 2.0$				$\gamma = 2.5$			
FRB	$\phi_0^{90\%}$	$F_\nu^{90\%}$	$E_{\rm min}$	$E_{\rm max}$	$\phi_0^{90\%}$	$F_\nu^{90\%}$	$E_{\rm min}$	$E_{\rm max}$	$\phi_0^{90\%}$	$F_\nu^{90\%}$	$E_{\rm min}$	$E_{\rm max}$
131104	1.6	1.3×10^3	5.8	7.9	1.1	8.80	3.4	6.8	0.4	13.5	2.6	5.5
140514	3.2	2.8×10^3	5.8	7.9	1.9	14.4	3.6	6.9	0.6	19.1	2.6	5.6
150215	2.9	2.6×10^3	5.8	7.9	2.3	17.7	3.1	6.5	0.4	15.8	2.4	5.0
150418	1.7	1.5×10^3	5.8	8.0	1.7	13.2	3.5	6.9	0.5	15.6	2.6	5.6
150807	0.4	3.4×10^2	5.8	8.0	1.6	12.1	3.6	6.9	0.9	25.1	2.6	5.7
151206	0.3	2.5×10^2	5.8	8.0	1.3	9.4	3.6	6.9	0.7	21.7	2.5	5.6
151230	1.0	8.9×10^2	5.8	8.0	1.6	12.8	3.2	6.8	0.5	17.1	2.4	5.2
160102	0.6	5.1×10^2	5.8	8.0	2.0	15.0	3.6	7.0	0.8	23.4	2.7	5.7
160317	3.1	2.7×10^3	5.8	7.9	1.6	12.8	3.5	6.9	0.4	14.9	2.5	5.5
160410	0.5	4.4×10^2	5.8	7.9	1.5	11.8	3.6	6.9	0.6	19.6	2.6	5.6
160608	1.7	1.5×10^3	5.8	7.9	2.1	16.3	3.6	7.0	0.6	18.5	2.7	5.7
170107	0.3	2.7×10^2	5.8	7.9	1.1	8.8	3.5	6.9	0.7	21.3	2.6	5.6

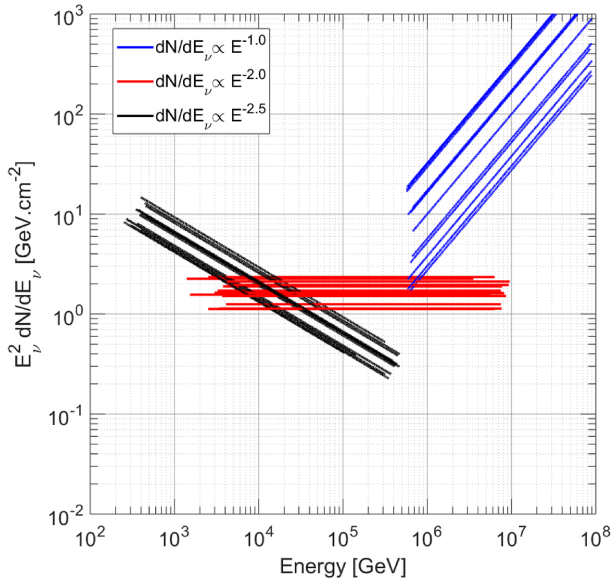

Figure 2. The 90 per cent confidence level ANTARES upper limits on the neutrino fluence for the power-law spectral models with $\gamma = 1.0$ (blue), 2.0 (red) and 2.5 (black), for each FRB. The limits are computed in the energy range [$E_{\rm min}$; $E_{\rm max}$] where 5–95 per cent of the neutrino signal is expected.

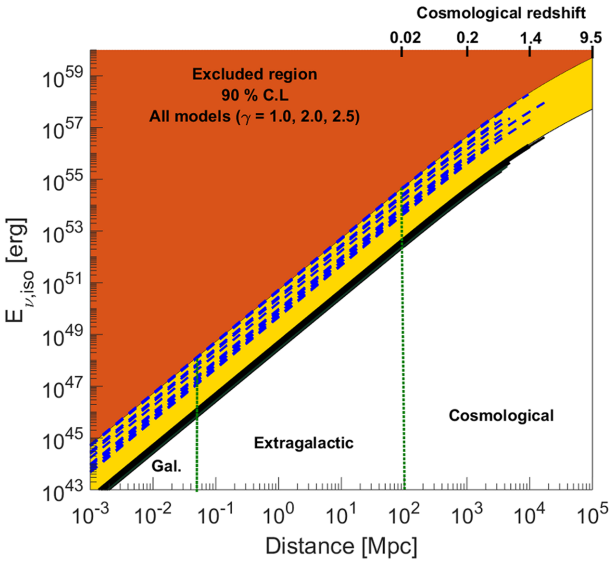

Figure 3. The 90 per cent confidence level upper limits on the neutrino energy released by the fast radio burst sources. The per-burst limits, assuming different neutrino power-law spectra, are shown with the dashed blue lines ($\gamma = 1.0$) and the black solid lines ($\gamma = 2.5$). These limits are computed in the distance range d $\in$ [1 kpc ; $D(z_{\rm DM})$]. The red area indicates the region that is already excluded by ANTARES at the 90 per cent confidence level for any considered hadronic model ($\gamma = 1.0, 2.0, 2.5$). The yellow area is only excluded by the soft spectral models ($\gamma = 2.0, 2.5$). The white area, divided into three distance scenarios, is still allowed according to the ANTARES sensitivity.

Galactic or very close to our Galaxy, typically up to the distance to the Magellanic Clouds, $d \leq 50$ kpc, (ii) extragalactic but non-cosmological, $d \in$ [50 kpc ; 100 Mpc] or (iii) cosmological, $d \geq 100$ Mpc. For these three ranges of distance, the upper limits on the neutrino fluence, see Fig. 3, can, for a $E_\nu^{-2.5}$ model, be converted to values in the source rest-frame by $E_{\nu,{\rm iso}}^{90\%} \leq$ [10^{43} ; 10^{46}], [10^{46} ; 10^{52}] and [10^{52} ; 10^{57}] erg, respectively.

4 DISCUSSION

The upper limits on the neutrino energy released by both the individual FRB sources and the whole population must be compared with the expectations of various FRB hadronic models.

4.1 Short-GRB progenitor

In the merger scenario, collapsing neutron stars may power an FRB at the merger time and then produce a short GRB a few seconds to hundreds of seconds later (Zhang 2014). In the standard framework of GRBs, particles are accelerated by internal shocks within the relativistic jetted outflow, and photo-hadronic processes may give rise to a burst of high-energy neutrinos (Waxman & Bahcall 1997; Guetta et al. 2004; Murase & Nagataki 2006; Zhang & Kumar 2013). The neutrino flux can be roughly scaled to the gamma-ray flux and to the baryonic load in the outflow according to (Zhang &

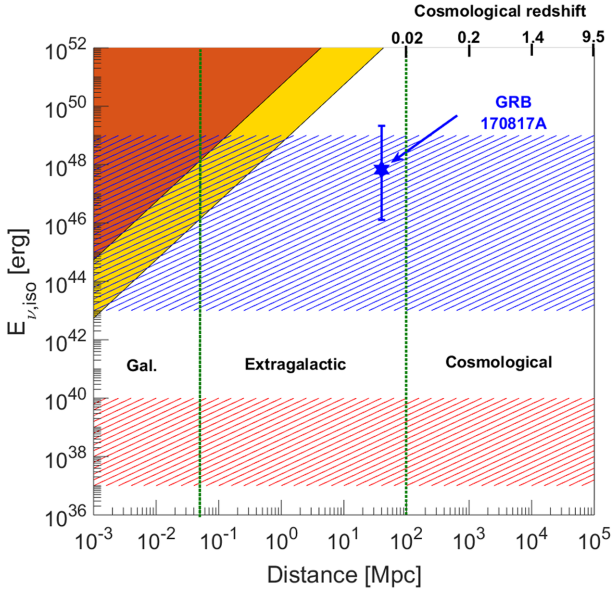

Figure 4. The $E_{\nu,iso}$−distance plane with the region already excluded by ANTARES for various neutrino models (red, $\gamma \geq 1.0$; yellow, $\gamma \geq 2.5$). The neutrino predictions from short gamma-ray bursts (GRBs) (standard internal shock model) are represented by the blue hatched region, while the magnetar/young neutron star neutrino flare expectations are represented by the red hatched area. The neutrino expectations for the short GRB GRB 170817A given by Biehl et al. (2018) are also shown. The errors result from the possible range for $f_p \in [1\,;1000]$.

Kumar 2013):

$$E_{\nu,\mathrm{iso}} \approx \frac{f_\mathrm{p}}{8}\left(1-(1-<\chi_{\mathrm{p}/\gamma}>)^{\tau_{\mathrm{p}\gamma}}\right) E_{\gamma,\mathrm{iso}}, \quad (6)$$

where f_p is the baryonic loading factor assumed to be preferentially in the range $f_\mathrm{p} \in [1\,;100]$, $\langle\chi_{\mathrm{p}/\gamma}\rangle \sim 20$ per cent is the fraction of the proton energy transferred to the pions, and $\tau_{\mathrm{p}\gamma}$ is the optical depth for photo-hadronic interactions (Albert et al. 2017d). For short GRBs, the isotropic gamma-ray energy released is usually in the range $E_{\gamma,\mathrm{iso}} \in [10^{47}; 10^{50}]$ erg. The short GRB 170817A associated with the binary neutron star merger event of 2017 August (Abbott et al. 2017a) was subluminous, with $E_{\gamma,\mathrm{iso}} = 3.1 \pm 0.7 \times 10^{46}$ erg integrated over an observed duration $T = (2 \pm 0.5)$ s (Abbott et al. 2017b). Typically, for a so-called standard short GRB,[3] the optical depth is $\sim 5 \times 10^{-2}$. Based on these rough estimates, the neutrino expectations are in the range $10^{-3} \times E_{\gamma,\mathrm{iso}} \lesssim E_{\nu,\mathrm{iso}} \lesssim 0.1 \times E_{\gamma,\mathrm{iso}}$. As shown in Fig. 4, the derived limits on the neutrino flux can rule out short-GRB models in located at very close distance ($d < 1$ kpc), assuming that the neutrinos are produced with an unbroken power-law spectrum. Our limits cannot constrain any model associating FRBs with short GRBs if the astrophysical sources are located at distances $d > 100$ Mpc. Recent advanced hadronic models imply a broken power-law spectrum for the neutrino emission in short-GRB events. Furthermore, the predictions from those models are weakly constrained by our exclusion regions. For instance, Biehl Heinze & Winter (2018) computed the expected neutrino spectrum from the short GRB GRB170817A using the NeuCosmA model (Hümmer et al. 2010; Hümmer, Baerwald & Winter 2012) for different configurations of the jetted outflow. Considering the low-luminosity jet scenario ($\Gamma = 30$, $f_p \in [1\,;1000]$), see fig. 2 in Biehl et al. (2018), the corresponding neutrino fluences integrated over 100 TeV–100 PeV are $F_\nu \in [4.3 \times 10^{-5}\,; 0.07]$ GeV cm^{-2}. At a distance of 40 Mpc and a redshift of $z = 0.008$, this translates into $E_{\nu,\mathrm{iso}} \in [10^{46}; 10^{49}]$ erg, which is still below the ANTARES sensitivity, as shown in Fig. 4.

[3]With the following parameters: the Lorentz factor $\Gamma = 300$, the gamma-ray energy $E_{\gamma,iso} \approx 10^{50}$ erg, the minimum variability time-scale of the gamma-ray emission $t_{\mathrm{var}} = 0.01$ s, the radius at which the pγ interactions occur $R_{\mathrm{p}\gamma} \approx 10^{13}$ cm, and the redshift $z = 0.5$.

4.2 Magnetar giant flare / soft gamma repeater (SGR)

In these two scenarios, the FRB event is produced by a sudden release of energy in the magnetosphere of the magnetar, driven either by magnetic instabilities or by high rotational loss (spin-down power). Protons may be accelerated into the polar cap regions and interact with the X-ray photon field emitted in the neutron star environment to produce high-energy neutrinos and secondary particles (Zhang et al. 2003). In the first scenario, the extremely strong magnetic field ($B > 10^{15}$ G) is the source of the X-ray photon field and of the particle acceleration. It corresponds to models of giant flares from magnetars or to SGR models. The second scenario is related to highly magnetized ($B \sim 10^{14}$ G) neutron stars that are born with a millisecond time-scale period of rotation, which enables them to power the particle acceleration and the subsequent high-energy neutrino emission (Dey et al. 2016). In both neutron star scenarios, a very high magnetic field is required, of at least $B > 10^{14}$ G. For a magnetar, the typical values for the stellar radius and the magnetic field used here are $B = 10^{15}$ G, $R = 10$ km. The rotational period, P, can vary from hundreds of milliseconds for a very young neutron star to a few seconds for slow-rotating magnetars (with $P > 2$ s). Based on these magnetar properties, the models of Zhang et al. (2003) and Dey et al. (2016) predict a high-energy neutrino luminosity in the range $L_{\nu,\mathrm{quiescent}} \in [10^{32}\,; 10^{35}]$ erg s^{-1} when the magnetar is in the quiescent state. For a giant flare like the one observed from SGR 1806-20 (Palmer et al. 2005), the luminosity of the X-ray/gamma-ray background (with $E_\gamma = 20$–30 keV; Zhang Xu & Qiao 2000) can increase by at least a factor of 10^6 in less than a second, compared with the quiescent periods of the magnetar (Thompson 2000). This kind of bursting event may also produce an FRB. By scaling the typical neutrino luminosity expected from quiescent magnetars to the SGR bursting events (with a typical duration for the main spike of $t_{\mathrm{spike}} \sim 0.1$ s; Thompson 2000; Palmer et al. 2005), one can obtain a rough estimate of the total energy released in neutrinos during giant flares from magnetars: $E_{\nu,iso} \leq 10^6 \times L_{\nu,\mathrm{quiescent}} \times t_{\mathrm{spike}} \leq [10^{37}; 10^{40}]$ erg.

These estimates are also compared, in Fig. 4, with the ANTARES neutrino upper limits. Magnetar/SGR sources are very probably weak sources of high-energy neutrinos according to the models depicted above. Hence the magnetar flare origin of FRBs cannot be significantly constrained on a per-burst basis with the neutrino analysis presented here.

4.3 Core collapse supernova environment

CCSNe are known to produce a compact object such as a neutron star or a black hole surrounded by the material ejected from the progenitor star during the explosion, the so-called supernova remnant. Murase & Nagataki (2006), Falcke & Rezzolla (2014), Ravi & Lasky (2014) and Li et al. (2014) mention the possibility that cosmic rays and high-energy neutrinos may be produced by the interaction of an energetic outflow ejected by the newly born compact object

with the surrounding pulsar nebula or supernova remnant at a distance $R \sim 10^{15-16}$ cm. An FRB could also be produced during this interaction or directly inside the ejected outflow. The resulting neutrino flux may be low, because at such a distance from the progenitor the density of the target medium for the photo-hadronic interaction is quite small. However, the delay between the production of the radio and the neutrino signal is not clear yet.

For all the hadronic models considered in this discussion, it seems that detecting a neutrino signal from single FRB sources may be difficult, as most of the FRB hadronic model predictions remain orders of magnitude below the ANTARES neutrino detection threshold. However, the expected large number of FRBs over the entire sky may contribute to a diffuse flux that can be tested by a large-scale neutrino telescope. This possibility is discussed in the following section.

4.4 Contribution to the neutrino diffuse flux

In 2013, the IceCube Collaboration reported the significant detection of a cosmic diffuse neutrino flux (Aartsen et al. 2013). To date, the sources responsible for this cosmic isotropic signal have not been clearly identified. Even though the first compelling evidence of a cosmic high-energy neutrino signal from the blazar TXS 0506 + 056 has been claimed by Aartsen et al. (2018a,b), it is still not clear how important the contribution of the blazars is to the neutrino diffuse flux. In contrast, the GRB contribution to this diffuse flux has already been constrained to be less than 1 per cent (Aartsen et al. 2015d). The population of FRBs may also contribute significantly, because their expected rate is high, $R_{\rm FRB} \sim 10^3\,{\rm d}^{-1}$ (Champion et al. 2016). This hypothesis is tested here by computing the 90 per cent CL upper limit on the diffuse neutrino flux associated with FRBs. As before, the neutrino flux associated with FRB sources is assumed to have a power-law energy distribution with spectral indexes $\gamma = 1.0, 2.0, 2.5$. The derived diffuse upper limits depend on the assumed neutrino spectrum. Hence,

$$E_\nu^2 \Phi_\nu^{90\%} = \frac{1}{4\pi}\,\phi_{\rm FRB}^{90\%}\,\frac{R_{\rm FRB}}{N_{\rm FRB}} \quad {\rm GeV\,cm^{-2}\,s^{-1}\,sr^{-1}}, \tag{7}$$

where $N_{\rm FRB}$ is the number of FRBs considered in this analysis and $\phi_{\rm FRB}^{90\%}$ is the characteristic neutrino fluence normalized to 100 TeV, as defined in equation (2) of the combined neutrino spectrum from the 12 FRBs. The neutrino fluence limit has been computed at the 90 per cent confidence level by estimating the average ANTARES effective area over the 12 FRB events for the different spectral models:

$$\phi_{\rm FRB}^{90\%} = \frac{2.3\,E_0^{-\gamma+2}}{\int \langle A_{\rm eff}(E_\nu)\rangle\,E_\nu^{-\gamma}\,{\rm d}E_\nu} \quad {\rm GeV\,cm^{-2}}. \tag{8}$$

According to the ANTARES upper limit on the individual neutrino fluxes from the 12 selected FRBs (see Table 2), and assuming the last updated estimate on the all-sky FRB rate $R_{\rm FRB} \sim 1.7 \times 10^3\,{\rm d}^{-1}$ (Bhandari et al. 2018), one can obtain the upper limits on the quasi-diffuse flux normalized to $E_0 = 100$ TeV, $E_\nu^2\phi_0^{90\%} < 0.9$, 2.0 and 0.7×10^{-4} GeV cm^{-2} s^{-1} sr^{-1} for $E^{-1.0}$, $E^{-2.0}$ and $E^{-2.5}$ neutrino spectra respectively.

The neutrino diffuse flux observed by the IceCube Collaboration for $E_\nu > 60$ TeV is at the level of $E_\nu^2\Phi_0 \sim 10^{-8}$ GeV cm^{-2} s^{-1} sr^{-1} normalized to $E_0 = 100$ TeV and with $\gamma = 2.46$ (Aartsen et al. 2015a). In the present analysis, the derived upper limit on the diffuse flux for FRBs with $\gamma = 2.5$ is above the signal measured by IceCube by a factor of ∼7300. This result is in agreement with the possibility that FRBs may originate from a wide variety of astrophysical progenitors, with few of them leading to hadronic processes in their environment. In addition, given the FRB rate mentioned above and the fact that on average one cosmic neutrino with $E_\nu > 60$ TeV is detected every 20 days by IceCube (Aartsen et al. 2015a), it appears that finally fewer than 1 over ∼20 000 FRB could be a detectable neutrino emitter. Nevertheless, according to the IceCube analysis, the number of cosmic neutrinos at lower energies is one or two orders of magnitude larger than those with $E_\nu > 60$ TeV, depending on the spectral index of the cosmic signal and the low-energy cut-off. These cosmic neutrinos at energies below 60 TeV are hidden in the IceCube data set within the much larger sample of atmospheric neutrinos. The possibility of observing a temporal and spatial coincidence allows for a significant suppression of this background. In this paper, a selection method is presented and guarantees the 3σ significance based on the observation of one coincident event. If the IceCube cosmic neutrino diffuse flux is produced exclusively by the mechanism that induces FRBs, accounting for the neutrinos below 60 TeV, the number of neutrinos per FRB can increase by one to two orders of magnitude. This means that searches for neutrinos with IceCube or ANTARES in coincidence with hundreds of FRBs could significantly constrain such a scenario. Alternatively, the non-detection of a neutrino signal from FRBs could be the result of non-hadronic production mechanisms in the FRB environment, or of the presence of a beamed jet of neutrinos.

Up to now, very few FRBs have been detected, which strongly limits the capability of large neutrino detectors to constrain the contribution of FRBs to the neutrino diffuse flux. In the near future, many radio facilities, for example UTMOST (Caleb et al. 2016, 2017; Bailes et al. 2017), SKA/ASKAP (Johnston et al. 2008; Bannister et al. 2017), CHIME (Bandura et al. 2014; Newburgh et al. 2014; Amiri et al. 2017) and Lofar (van Leeuwen 2014; Maan & van Leeuwen 2017) will increase the statistics of FRB detection up to a few per year to several hundreds per year. In the meantime, bright and very close events may be also detected (by CHIME and ASKAP, for instance) which will also increase the discovery capabilities of the large-scale neutrino detectors for individual point sources.

4.5 The complementarity of the ANTARES and IceCube detectors for FRB searches

A similar search for high-energy neutrinos from FRBs has been performed by the IceCube Collaboration (Aartsen et al. 2018c). Despite the larger detection volume with respect to the ANTARES telescope, no significant signal was found. The IceCube neutrino telescope is sensitive mostly to FRBs occurring in the Northern hemisphere, where the derived upper limits on the neutrino fluence for a E^{-2} spectrum are about a factor 20 more stringent than those determined by ANTARES at its maximum sensitivity (obtained for sources located in the Southern sky). However, the IceCube effective area is greatly reduced for declination $\delta < -20^\circ$ with respect to positive declinations. Therefore, in the Southern sky, where to date most of the FRBs have been detected, the ANTARES telescope is still competitive with IceCube to constrain models that assume a soft spectral index such as $\gamma = 2.5$. In the Southern sky, the strongest upper limit on the neutrino fluence given by ANTARES for an FRB is a factor ∼1.3 better than the one given by IceCube (see fig. 7 in Aartsen et al. 2018c). Indeed, the effective area of ANTARES described in this analysis is larger than that of IceCube below $E_\nu \lesssim 25$ TeV for two-thirds of the Southern sky and

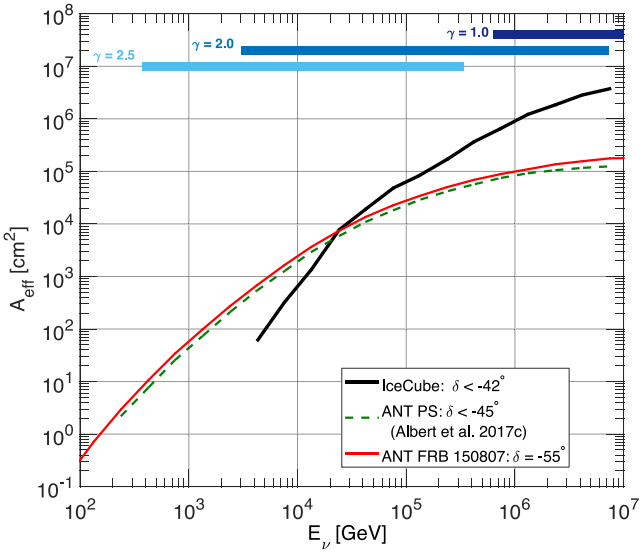

Figure 5. The ANTARES and IceCube effective areas ($A_{\rm eff}$) as a function of the neutrino energy. The dashed dark green line is the ANTARES $A_{\rm eff}$ computed as for the standard point-source neutrino searches in ANTARES data at a declination of $\delta < -45^\circ$ (Albert et al. 2017c). The red line illustrates the gain of about 30 per cent in the $A_{\rm eff}$ ($\delta = -55^\circ$) typically achievable when searching for a transient event, such as the FRBs presented in this paper. The IceCube $A_{\rm eff}$ computed in the last FRB analysis (Aartsen et al. 2018c) in the same range of Southern declinations is represented with the black line.

in the large portion of the energy range where 90 per cent of the neutrino signal is expected for $\gamma = 2.5$. In Fig. 5, the ANTARES $A_{\rm eff}$ computed at a declination $\delta = -55^\circ$ for FRB 150807 is compared with the IceCube $A_{\rm eff}$ computed for FRB searches in the declination range $\delta \in [-90^\circ; -42^\circ]$ (Aartsen et al. 2018c) and illustrates the synergy between IceCube and ANTARES in terms of sky and energy coverages. Thus, in the Southern hemisphere, the use of both the ANTARES and the IceCube neutrino telescopes to search for transient events with soft spectra, such as the one observed for the neutrino cosmic diffuse flux, maximizes the discovery potential.

Despite the good performances of IceCube for hard neutrino spectra (the high-energy part of the spectrum) in the Southern sky (see Fig. 5), a larger detector than ANTARES located in the Northern hemisphere is required to improve the sensitivity of the neutrino telescopes to sources located in the Southern hemisphere. The next generation of the large-scale[4] high-energy neutrino detector, KM3NeT/ARCA (Adrián-Martínez et al. 2016), is now under construction in the Mediteranean Sea and will be fully operational in the upcoming years. With KM3NeT/ARCA, an unprecedented sensitivity to the high-energy neutrino flux should be obtained at Southern declinations. In the next few years, combined analysis with the KM3NeT/ARCA and the IceCube detectors will provide the most sensitive and homogeneous coverage of the neutrino sky ever reached for energies $E_\nu > 1$ TeV.

5 CONCLUSIONS

FRBs are candidate sources of efficient particle acceleration because they could release large amounts of energy on short time-scales, similar to short GRBs. The question whether a hadronic component is injected in the energetic outflow has been investigated in this paper by directly searching for high-energy neutrinos in coincidence with 12 FRBs using ANTARES data in the period 2013–2017. No significant coincident neutrino signal was found. The 90 per cent CL upper limits on the neutrino fluence have been derived per burst and for the whole population, as well as the neutrino energy released. These limits are not stringent enough to significantly constrain the prediction of some FRB hadronic models, for example merger events and magnetar flares, especially if these sources are located at cosmological distances. FRBs could be weak sources of high-energy neutrinos, but because of their high rate in the Universe, the signal from the whole population may be detectable as a diffuse neutrino flux. To date, the lack of FRB statistics does not allow this hypothesis to be firmly tested, because the detection of at least a hundred FRBs is required in order to bring significant constraints. The upcoming first observations from KM3NeT/ARCA, a next-generation, large-scale, high-energy neutrino telescope in the Northern hemisphere, will also permit a significant improvement in the constraints on the fluence per burst and the FRB contribution to the cosmic neutrino diffuse flux. Recently, new facilities such as UTMOST, CHIME and SKA/ASKAP have emerged, with high discovery capabilities of tens of FRBs per month (against ∼3–4 per year during the last 10 years) and covering more than just the Southern sky. These new radio facilities will allow to exploit the current and future neutrino detector capabilities: for FRBs detected in the northern sky with IceCube and IceCube-Gen2 detectors and in the Southern sky with ANTARES and KM3NeT/ARCA (note also that the KM3NeT/ARCA dectector should have at least comparable performances with the current IceCube detector in the Northern sky for declinations $\delta \lesssim +40^\circ$). In addition, these radio facilities may be able to observe bright FRBs at close distances ($d = 100$ Mpc), which will enhance the probabilty of a multimessenger detection at high energies for an individual FRB. Finally, more accurate models describing the neutrino production associated with FRBs will greatly help to refine the constraints on the neutrino fluence and energy released.

ACKNOWLEDGEMENTS

The authors acknowledge financial support from the following funding agencies: Centre National de la Recherche Scientifique (CNRS), Commissariat à l'énergie atomique et aux énergies alternatives (CEA), Commission Européenne (FEDER fund and Marie Curie Program), Institut Universitaire de France (IUF), IdEx program and UnivEarthS Labex program at Sorbonne Paris Cité (ANR-10-LABX-0023 and ANR-11-IDEX-0005-02), Labex OCEVU (ANR-11-LABX-0060) and the A*MIDEX project (ANR-11-IDEX-0001-02), Région Île-de-France (DIM-ACAV), Région Alsace (contrat CPER), Région Provence-Alpes-Côte d'Azur, Département du Var and Ville de La Seyne-sur-Mer, France; Bundesministerium für Bildung und Forschung (BMBF), Germany; Istituto Nazionale di Fisica Nucleare (INFN), Italy; Stichting voor Fundamenteel Onderzoek der Materie (FOM), Nederlandse organisatie voor Wetenschappelijk Onderzoek (NWO), the Netherlands; Council of the President of the Russian Federation for young scientists and leading scientific schools supporting grants, Russia; National Authority for Scientific Research (ANCS), Romania; Ministerio de Economía y Competitividad (MINECO): Plan Estatal de Investigación (refs. FPA2015-65150-C3-1-P, -2-P and -3-P, (MINECO/FEDER)), Severo Ochoa Centre of Excellence and MultiDark Consolider (MINECO), and Prometeo and Grisolía pro-

[4]With a detection volume of the order of km^3.

grams (Generalitat Valenciana), Spain; Ministry of Higher Education, Scientific Research and Professional Training, Morocco. We also acknowledge technical support from Ifremer, AIM and Foselev Marine for the sea operation and CC-IN2P3 for the computing facilities.

REFERENCES

Aartsen M. G. et al., 2013, Phys. Rev. Lett., 111, 021103
Aartsen M. G. et al., 2015a, Phys. Rev. D, 91, 022001
Aartsen M. G. et al., 2015b, preprint (arXiv:1510.05223)
Aartsen M. G. et al., 2015c, ApJ, 809, 98
Aartsen M. G. et al., 2015d, ApJ, 805, L5
Aartsen M. G. et al., 2016, ApJ, 833, 3
Aartsen M. G. et al., 2018a, Science, 361, 1378
Aartsen M. G. et al., 2018b, Science, 361, 147
Aartsen M. G. et al., 2018c, ApJ, 875, 117
Abbott B. P. et al., 2017a, Phys. Rev. Lett., 119, 161101
Abbott B. P. et al., 2017b, ApJ, 848, L13
Ade P. A. R. et al., 2016, A&A, 594, A13
Adrián-Martínez S. et al., 2012, ApJ, 760, 53
Adrián-Martínez S. et al., 2016, J. Phys. G Nucl. Phys., 43, 084001
Ageron M. et al., 2011, Nucl. Inst. Meth. Physic. Res. A, 656, 11
Albert A. et al., 2017a, preprint(arXiv:1711.01486)
Albert A. et al., 2017b, Eur. Phys. J. C, 77, 911
Albert A. et al., 2017c, Phys. Rev. D, 96, 082001
Albert A. et al., 2017d, MNRAS, 469, 906
Albert A. et al., 2018, ApJ, 853, L7
Amiri M. et al., 2017, preprint (arXiv:1702.08040)
Bailes M. et al., 2017, Publ. Astron. Soc. Aust., 34, e045
Bandura K. et al., 2014, in Proc. SPIE, Vol. 9145, Ground-based and Airborne Telescopes V, SPIEp. 914522
Bannister K. W. et al., 2017, ApJ, 841, L12
Bhandari S. et al., 2018, MNRAS, 475, 1427
Biehl D., Heinze J., Winter W., 2018, MNRAS, 476, 1191
Bietenholz M. F., Bartel N., 2017, ApJ, 851, 2017
Caleb M. et al., 2016, MNRAS, 458, 718
Caleb M. et al., 2017, MNRAS, 468, 3746
Cao X.-F., Yu W.-Y, 2018, Phys. Rev. D, 97, 023022
Champion D. J. et al., 2016, MNRAS, 460, L30
Chatterjee S. et al., 2017, Nature, 541, 58
Cordes J. M., Wasserman I., 2016, MNRAS, 457, 232
DeLaunay J. J. et al., 2016, ApJ, 832, L1
Dey R. K., Ray S., Dam S., 2016, EPL (Europhys. Lett.), 115, 69002
Fahey S., Kheirandish A., Vandenbroucke J., Xu D., 2017, ApJ, 845, 14
Falcke H., Rezzolla L., 2014, A&A, 562, A137
Goldstein A. et al., 2013, ApJS, 208, 21
Guetta D., Hooper D., Alvarez-Mun∼Iz J., Halzen F., Reuveni E., 2004, Astropart. Phys., 20, 429
Hardy L. K. et al., 2017, MNRAS, 472, 2800
Hümmer S., Rüger M., Spanier F., Winter W., 2010, ApJ, 721, 630
Hümmer S., Baerwald P., Winter W., 2012, Phys. Rev. Lett., 108, 231101
Johnston S. et al., 2008, Exp. Astron., 22, 151
Katz J. I., 2014, Phys. Rev. D, 89, 103009
Keane E. F. et al., 2016, Nature, 530, 453
Li X., Zhou B., He H.-N., Fan Y.-Z., Wei D.-M., 2014, ApJ, 797, 33
Lorimer D., Kramer M., 2005, Book Review: Handbook of Pulsar Astronomy. The Observatory, Vol. 125. Cambridge Univ. Press, Cambridgep. 338
Lorimer D. R., Bailes M., McLaughlin M. A., Narkevic D. J., Crawford F., 2007, Science, 318, 777
Lyubarsky Y., 2014, MNRAS, 442, L9
Maan Y., van Leeuwen J., 2017, preprint (arXiv:1709.06104)
Marcote B. et al., 2017, ApJ, 834, L8
Murase K., Nagataki S., 2006, Phys. Rev. D, 73, 063002
Murase K., Kashiyama K., Mészáros P., 2016, MNRAS, 461, 1498
Murase K., Mészáros P., Fox D. B., 2017, ApJ, 836, L6
Newburgh L. B. et al., 2014, in Proc. SPIE, Vol. 9145, Ground-based and Airborne Telescopes V, SPIE, Montréal, Quebec, Canada. p. 91454V
Palaniswamy D. et al., 2014, ApJ, 790, 63
Palmer D. M. et al., 2005, Nature, 434, 1107
Patel C. et al., 2018, preprint(arXiv:1808.03710)
Pen U.-L., Connor L., 2015, ApJ, 807, 179
Petroff E. et al., 2015a, MNRAS, 454, 457
Petroff E. et al., 2015b, MNRAS, 447, 246
Petroff E. et al., 2016, Publ. Astron. Soc. Aust., 33, e045
Petroff E. et al., 2017, MNRAS, 469, 4465
Popov S. B., Postnov K. A., 2010, in Harutyunian H. A., Mickaelian A. M., Terzian Y., eds, Evolution of Cosmic Objects through their Physical Activity, Gitutyun Publishing House of NAS RA. p. 129
Popov S. B., Postnov K. A., 2013, preprint(arXiv:1307.4924)
Ravi V., Lasky P. D., 2014, MNRAS, 441, 2433
Ravi V., Shannon R. M., Jameson A., 2015, ApJ, 799, L5
Scholz P. et al., 2016, ApJ, 833, 177
Scholz P. et al., 2017, ApJ, 846, 80
Spitler L. G. et al., 2016, Nature, 531, 202
Tendulkar S. P. et al., 2017, ApJ, 834, L7
Thompson C., 2000, in Kramer M., Wex N., Wielebinski R., eds, ASP Conf. Ser. Vol. 202, IAU Colloq. 177: Pulsar Astronomy – 2000 and Beyond, Astron. Soc. Pac., San Francisco. p. 669
Thornton D. et al., 2013, Science, 341, 53
Totani T., 2013, Pub. Astron. Soc. Japan, 65, L12
van Leeuwen J., 2014, The Third Hot-wiring the Transient Universe Workshop. p. 79, Available at: cdsads.u-strasbg.fr/abs/2014htu..conf...79VCE
Wang J.-S., Yang Y.-P., Wu X.-F., Dai Z.-G., Wang F.-Y., 2016, ApJ, 822, L7
Waxman E., Bahcall J., 1997, Phys. Rev. Lett., 78, 2292
Ye J., Wang K., Cai Y.-F., 2017, Eur. Phys. J. C, 77, 720
Zhang B., 2014, ApJ, 780, L21
Zhang B., Kumar P., 2013, Phys. Rev. Lett., 110, 121101
Zhang B., Xu R. X., Qiao G. J., 2000, ApJ, 545, L127
Zhang B., Dai Z. G., Mészáros P., Waxman E., Harding A. K., 2003, ApJ, 595, 346

[1]*Université de Strasbourg, CNRS, IPHC UMR 7178, F-67000 Strasbourg, France*
[2]*Technical University of Catalonia, Laboratory of Applied Bioacoustics, Rambla Exposició, 08800 Vilanova i la Geltrú, Barcelona, Spain*
[3]*INFN – Sezione di Genova, Via Dodecaneso 33, 16146 Genova, Italy*
[4]*Friedrich-Alexander-Universität Erlangen-Nürnberg, Erlangen Centre for Astroparticle Physics, Erwin-Rommel-Strasse 1, 91058 Erlangen, Germany*
[5]*Institut d'Investigació per a la Gestió Integrada de les Zones Costaneres (IGIC) – Universitat Politècnica de València, C/ Paranimf 1, 46730 Gandia, Spain*
[6]*Aix Marseille Université, CNRS/IN2P3, CPPM, Marseille, France*
[7]*APC, Université Paris Diderot, CNRS/IN2P3, CEA/Irfu, Obs de Paris, Sorbonne Paris Cité, France*
[8]*IFIC – Instituto de Física Corpuscular (CSIC – Universitat de València), c/ Catedrático José Beltrán, 2 E-46980 Paterna, Valencia, Spain*
[9]*LAM – Laboratoire d'Astrophysique de Marseille, Pôle de l'Étoile Site de Château-Gombert, rue Frédéric Joliot-Curie 38, 13388 Marseille Cedex 13, France*
[10]*National Center for Energy Sciences and Nuclear Techniques, B.P.1382, R. P.10001 Rabat, Morocco*
[11]*INFN – Laboratori Nazionali del Sud (LNS), Via S. Sofia 62, 95123 Catania, Italy*
[12]*Nikhef, Science Park, Amsterdam, the Netherlands*
[13]*Huygens-Kamerlingh Onnes Laboratorium, Universiteit Leiden, the Netherlands*
[14]*University Mohammed V in Rabat, Faculty of Sciences, 4 av. Ibn Battouta, BP 1014, RP 10000 Rabat, Morocco*
[15]*Institute of Space Science, RO-077125 Bucharest, Măgurele, Romania*
[16]*Universiteit van Amsterdam, Instituut voor Hoge-Energie Fysica, Science Park 105, 1098 XG Amsterdam, the Netherlands*

[17]*INFN – Sezione di Roma, P.le Aldo Moro 2, 00185 Roma, Italy*
[18]*Dipartimento di Fisica dell'Università La Sapienza, P.le Aldo Moro 2, 00185 Roma, Italy*
[19]*Gran Sasso Science Institute, Viale Francesco Crispi 7, 00167 L'Aquila, Italy*
[20]*LPHEA, Faculty of Science – Semlali, Cadi Ayyad University, POB 2390, Marrakech, Morocco*
[21]*INFN – Sezione di Bologna, Viale Berti-Pichat 6/2, 40127 Bologna, Italy*
[22]*INFN – Sezione di Bari, Via E. Orabona 4, 70126 Bari, Italy*
[23]*Department of Computer Architecture and Technology/CITIC, University of Granada, 18071 Granada, Spain*
[24]*Géoazur, UCA, CNRS, IRD, Observatoire de la Côte d'Azur, Sophia Antipolis, France*
[25]*Dipartimento di Fisica dell'Università, Via Dodecaneso 33, 16146 Genova, Italy*
[26]*Université Paris-Sud, 91405 Orsay Cedex, France*
[27]*University Mohammed I, Laboratory of Physics of Matter and Radiations, BP 717, Oujda 6000, Morocco*
[28]*Institut für Theoretische Physik und Astrophysik, Universität Würzburg, Emil-Fischer Strasse 31, 97074 Würzburg, Germany*
[29]*Dipartimento di Fisica e Astronomia dell'Università, Viale Berti Pichat 6/2, 40127 Bologna, Italy*
[30]*Laboratoire de Physique Corpusculaire, Clermont Université, Université Blaise Pascal, CNRS/IN2P3, BP 10448, F-63000 Clermont-Ferrand, France*
[31]*LIS, UMR Université de Toulon, Aix Marseille Université, CNRS, 83041 Toulon, France*
[32]*Royal Netherlands Institute for Sea Research (NIOZ) and Utrecht University, Landsdiep 4, 1797 SZ 't Horntje (Texel), the Netherlands*
[33]*Institut Universitaire de France, 75005 Paris, France*
[34]*Dr Remeis-Sternwarte and ECAP, Friedrich-Alexander-Universität Erlangen-Nürnberg, Sternwartstrasse 7, 96049 Bamberg, Germany*
[35]*Moscow State University, Skobeltsyn Institute of Nuclear Physics, Leninskie gory, 119991 Moscow, Russia*
[36]*Mediterranean Institute of Oceanography (MIO), Aix-Marseille Université, 13288 Marseille, Cedex 9, France; Université du Sud Toulon-Var, CNRS-INSU/IRD UM 110, 83957, La Garde Cedex, France*
[37]*INFN – Sezione di Catania, Via S. Sofia 64, 95123 Catania, Italy*
[38]*Direction des Sciences de la Matière – Institut de recherche sur les lois fondamentales de l'Univers – Service de Physique des Particules, CEA Saclay, 91191 Gif-sur-Yvette Cedex, France*
[39]*INFN – Sezione di Pisa, Largo B. Pontecorvo 3, 56127 Pisa, Italy*
[40]*Dipartimento di Fisica dell'Università, Largo B. Pontecorvo 3, 56127 Pisa, Italy*
[41]*INFN – Sezione di Napoli, Via Cintia, 80126 Napoli, Italy*
[42]*Dipartimento di Fisica dell'Università Federico II di Napoli, Via Cintia, 80126, Napoli, Italy*
[43]*Departamento de Física Teórica y del Cosmos & CAFPE, University of Granada, 18071 Granada, Spain*
[44]*GRPHE – Université de Haute Alsace – Institut universitaire de technologie de Colmar, 34 rue du Grillenbreit, BP 50568 – 68008 Colmar, France*

This paper has been typeset from a TEX/LATEX file prepared by the author.